Journal of Cerebral Blood Flow and Metabolism
11:898–913 © 1991 The International Society of Cerebral Blood Flow and Metabolism
Published by Raven Press, Ltd., New York

Kinetics and Modeling of L-6-[^{18}F]Fluoro-DOPA in Human Positron Emission Tomographic Studies

Sung-cheng Huang, Dan-chu Yu, Jorge R. Barrio, Scott Grafton, William P. Melega, John M. Hoffman, N. Satyamurthy, John C. Mazziotta, and Michael E. Phelps

Division of Nuclear Medicine, Department of Radiological Sciences, and Laboratory of Nuclear Medicine, Laboratories of Biomedical and Environmental Sciences, UCLA School of Medicine, University of California at Los Angeles, Los Angeles, California, U.S.A.

Summary: Kinetics of L-3,4-dihydroxy-6-[^{18}F]fluorophenylalanine (FDOPA) in striatum and cerebellum were measured in 10 normal human subjects with positron emission tomography (PET) from 0 to 120 min after an intravenous bolus injection of the tracer. The time course of the arterial plasma concentrations of the tracer and its metabolites was also assayed biochemically. FDOPA compartmental models that are based on biochemical information were investigated for their consistency with the measured striatal and cerebellar tissue kinetics. A modeling approach was also developed for separating plasma FDOPA and metabolite time-activity curves from the measured total ^{18}F time-activity curve in plasma. Results showed that a model consisting of three separate compartments for tissue FDOPA, tissue 6-[^{18}F]fluorodopamine (FDA) and its metabolites, and tissue L-3,4-dihydroxy-6-[^{18}F]fluoro-3-*O*-methylphenylalanine (3-OMFD) could describe adequately the striatal kinetics in humans. Based on this model, the FDOPA transport constant across the blood–brain barrier (BBB) (K_1), the FDOPA decarboxylation rate constant (k_3), and the turnover rate constant of FDA and its metabolites (k_4) could be estimated by model fitting to the tissue kinetics and were found for the normal subjects to be 0.031 ± 0.006 ml/min/g (mean ± SD), 0.041 ± 0.015/min, and 0.004 ± 0.002/min, respectively. About 50% of the FDOPA that crossed the BBB from plasma to striatum was decarboxylated. The decarboxylation constant with respect to plasma FDOPA (K_3) was 0.015 ± 0.003 ml/min/g. The BBB transport corresponded to a permeability–surface area product of 0.032 ml/min/g for FDOPA. For 3-OMFD, the BBB transport was 1.7 times faster. The effects of tissue heterogeneity on the FDOPA kinetics and on the estimated model parameters were also investigated. The usefulness and implications of these findings for interpretation of PET FDOPA studies are discussed. **Key Words:** Blood–brain transport—Blood time–activity curve—Cerebellum—L-3,4-Dihydroxy-6-[^{18}F]fluorophenylalanine—L-3,4-Dihydroxy-6-[^{18}F]fluoro-3-*O*-methylphenylalanine turnover rate—Striatum.

L-3,4-Dihydroxy-6-[^{18}F]fluorophenylalanine (FDOPA) has been widely used with positron emission tomography (PET) to examine changes in the presynaptic dopaminergic function in animals and humans (Garnett et al., 1983*a*, 1984; Calne et al., 1985; Nahmias et al., 1985; Chiueh et al., 1986; Firnau et al., 1986; Martin et al., 1986, 1989; Guttman et al., 1987, 1989; Leenders et al., 1987, 1988; Freed et al., 1990; Lindvall et al., 1990). In normal subjects, the tracer is converted to 6-[^{18}F]fluorodopamine (FDA) by aromatic amino acid decarboxylase (AAAD) and retained in the striatum. FDOPA uptake is decreased in patients with Parkinson's disease or with *N*-methyl-4-phenyl-1,2,3,6-tetrahydropyridine-induced degeneration of the nigrostriatal pathway. Therefore, the uptake of the tracer in the striatal region has been useful for indicating the presynaptic integrity of dopaminergic neurons (Barrio et al., 1988). The interpretation of the results, however, has been mostly by qualitative examination of the relative radioactivity distribution in the brain

Received December 12, 1990; revised May 6, 1991; accepted May 10, 1991.

Address correspondence and reprint requests to Dr. S.-C. Huang at Division of Nuclear Medicine, Department of Radiological Sciences, UCLA School of Medicine, 405 Hilgard Ave., Los Angeles, CA 90024, U.S.A.

Abbreviations used: AAAD, aromatic amino acid decarboxylase; BBB, blood–brain barrier; FDA, 6-[^{18}F]fluorodopamine; FDOPA, L-3,4-dihydroxy-6-[^{18}F]fluorophenylalanine; FDOPAC, 6-[^{18}F]fluoro-3,4-dihydroxyphenylacetic acid; FHVA, 6-[^{18}F]fluorohomovanillic acid; 3-OMFD, L-3,4-dihydroxy-6-[^{18}F]fluoro-3-*O*-methylphenylalanine; PET, positron emission tomography.

(Garnett et al., 1983*a,b,* 1984; Calne et al., 1985; Guttman et al., 1989). One important feature of FDOPA kinetics is that the tracer is rapidly converted systemically to L-3,4-dihydroxy-6-[^{18}F]fluoro-3-*O*-methylphenylalanine (3-OMFD) (Boyes et al., 1986; Cumming et al., 1987; Firnau et al., 1987; Melega et al., 1990*a*) that in turn can cross the blood–brain barrier (BBB) and contribute to the total radioactivity measured in cerebral tissue. This complicates the interpretation of PET images, in which only the total radioactivity concentration in local tissue regions can be measured.

Early quantitative studies have used the radioactivity ratio between striatum and cerebellum (or background) at 60–120 min after FDOPA injection as an index to differentiate between normals and patients (Calne et al., 1985; Leenders et al., 1986*a;* Martin et al., 1986; Doudet et al., 1989). In some studies, the background activity level (cerebellum) has been subtracted from the striatal activity before taking the ratio to minimize the effect of 3-OMFD in tissue (Guttman et al., 1989). The striatum/cerebellum ratio of ^{18}F concentration has been shown to increase approximately at a constant rate after the time of injection (Leenders et al., 1986*b*). Modeling analysis has been applied to show that plots of this ratio versus the normalized time (Patlak et al., 1983), using either the cerebellar time–activity curve or the total blood activity curve as the input function, are approximately linear (Leenders et al., 1989; Lindvall et al., 1990; Tedroff et al., 1990). The Patlak graphical method has also been formally applied to analyze FDOPA data (Martin et al., 1989) using the plasma FDOPA curve as the input function to give the uptake constant of FDOPA from plasma to striatum. In contrast to earlier analyses, this last approach explicitly accounted for 3-OMFD in plasma and in tissue.

The uptake constant of FDOPA obtained by this approach, however, is not specific to the AAAD activity in striatal tissue, because the uptake could be affected directly by changes in the transport mechanism across the BBB. Also, although a general model based on the biochemical pathways of FDOPA has been used in the last two methods reviewed above, the model has not been fully investigated for its adequacies and limitations in describing FDOPA kinetics in the striatum.

A well-characterized model for the kinetics of FDOPA can enhance our understanding of the PET measurements and in turn can lead to the development of more reliable techniques for analyzing and interpreting results from FDOPA studies (Huang et al., 1989; Yu et al., 1990). An FDOPA model had been examined previously (Garnett et al., 1980), but with kinetic data obtained from monkey studies in which an external scintillation detector was used. These measurements were more representative of the kinetics in the extracerebral and nonstriatal cerebral tissues than of striatal tissues. The results, therefore, have not been utilized for the analysis of FDOPA PET data. Recently, an FDOPA model based on known biochemical information about the tracer has been used for analyzing FDOPA kinetics in rat (Reith et al., 1990). The model, however, has not been directly verified in terms of its adequacy to describe the kinetics of FDOPA in cerebral tissue.

In this study, we perform dynamic PET studies of FDOPA in normal human subjects to assess human striatal FDOPA kinetics. We investigate the model configuration that best describes these kinetics and is consistent with quantitative biochemical information known for this tracer (Melega et al. 1991*a,b*). This model demonstrates the feasibility of measuring the turnover rate constant of FDA and its metabolites in tissue with PET. A new approach to separate the time–activity curves of FDOPA and its labeled metabolites is also introduced. The characteristics of the model in terms of the reliability of the estimate of the model parameters are presented.

THEORY

Figure 1 illustrates the various transport and biochemical pathways of FDOPA in the human body. The tracer is assumed to have access to bidirectional transport across the BBB. The transport mechanism is the neutral amino acid carrier in the BBB (Oldendorf, 1971). In striatum, FDOPA is decarboxylated to FDA by AAAD in presynaptic dopaminergic terminals. Similar to dopamine, FDA will be released from these neurons into the synaptic cleft and can be transported back into neurons' reuptake sites. FDA can also be metabolized to 6-[^{18}F]fluoro-3,4-dihydroxyphenylacetic acid (FDOPAC) and 6-[^{18}F]fluorohomovanillic acid (FHVA), which in turn can cross the BBB and be cleared from tissue by venous blood flow. Plasma FDOPA is also converted to 3-OMFD in the periphery, such as the liver, kidney, and the red blood cell, and appears rapidly in plasma (Cumming et al., 1987; Firnau et al., 1987; Melega et al., 1990*a*). 3-OMFD can cross the BBB through the neutral amino acid carrier as does FDOPA, but probably with a different permeability. 3-OMFD of peripheral origin is assumed not to participate in any biochemical reactions in brain tissues and the rate of direct conversion from FDOPA to 3-OMFD in striatum is assumed small and negligible. Similar trans-

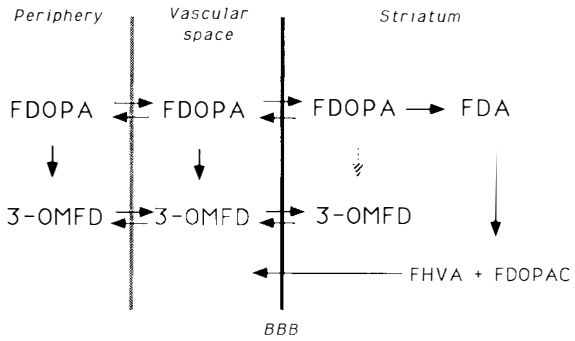

FIG. 1. Schematic diagram illustrating the various transport and biochemical pathways of FDOPA in the human body. The tracer is assumed transportable across the BBB bidirectionally. In striatum, FDOPA is decarboxylated to FDA by AAAD in presynaptic dopaminergic neurons. FDA can be metabolized to FDOPAC and FHVA, which in turn can cross the BBB and be cleared from tissue by venous blood flow. Plasma FDOPA can also be converted to 3-OMFD in the periphery. 3-OMFD can cross the BBB, but is assumed not to participate in any biochemical reactions in brain tissues. The rate of direct conversion from FDOPA to 3-OMFD in striatum is assumed small and negligible. Similar transport pathways are assumed for FDOPA and 3-OMFD in cerebellum, except that FDOPA is not converted to FDA in cerebellum. If carbidopa is not given to the subject, FDOPA in the periphery could also be converted to FDA, the conjugates of which can go back to the plasma (not shown in the figure). For abbreviations see the text.

port properties are assumed for FDOPA and 3-OMFD in cerebellum, except that FDOPA is not converted to FDA as determined by biochemical assay of cerebellar tissue (Melega et al., 1991*a*,*b*).

Models for FDOPA in striatum and cerebellum

Based on the above information, compartmental models for the tracer in striatum and cerebellum can be configured as shown in Fig. 2A and B. For striatum, the model consists of separate compartments for tissue FDOPA, tissue 3-OMFD, and FDA (and its metabolites). The ^{18}F radioactivity concentrations in the three compartments are denoted, respectively, as C_1, C_2, and C_3; K_1 and k_2 are the forward and reverse transport rate constants of plasma FDOPA to the tissue FDOPA compartment; k_3 is the rate constant from the tissue FDOPA compartment to the combined compartment of FDA and its metabolites; k_4 is the clearance rate constant of ^{18}F out of the tissue to plasma from the compartment of FDA and its metabolites; K_5 and k_6 are, respectively, the forward and reverse transport rate constants of plasma 3-OMFD to the tissue 3-OMFD compartment. According to this model, the striatal ^{18}F concentration $[C_s(t)]$ at time t can be expressed as

$$\begin{aligned} C_s(t) = {} & K_1 C_{fd}(t) * \exp[-(k_2 + k_3)t] \\ & + K_1 k_3 C_{fd}(t) * \exp[-(k_2 + k_3)t] \\ & * \exp(-k_4 t) + C_{omfd}(t) * K_5 \exp(-k_6 t) \\ & + CBV \cdot C_{wb}(t) \end{aligned} \quad (1)$$

where C_{fd} and C_{omfd} are, respectively, the radioactivity concentrations of FDOPA and 3-OMFD in plasma; $C_{wb}(t)$ is the ^{18}F concentration in whole blood; CBV denotes the blood volume in tissue; and the symbol * denotes the mathematical operation of convolution. The time average striatal radioactivity (C_{sm}) corresponding to a PET measurement over a scan interval from t_1 to t_2 can then be expressed as

$$C_{sm}(t_1;t_2) = \frac{\int_{t_1}^{t_2} C_s(t)dt}{t_2 - t_1} \quad (2)$$

As shown in Fig. 2B, the model for cerebellum is similar to that for striatum, except that there is no compartment for FDA and that k_3 is zero. A subscript "p" is added to each notation for the cerebellar model to distinguish them from those of the striatal model. The total ^{18}F concentration in cerebellum $[C_c(t)]$ can then be expressed as

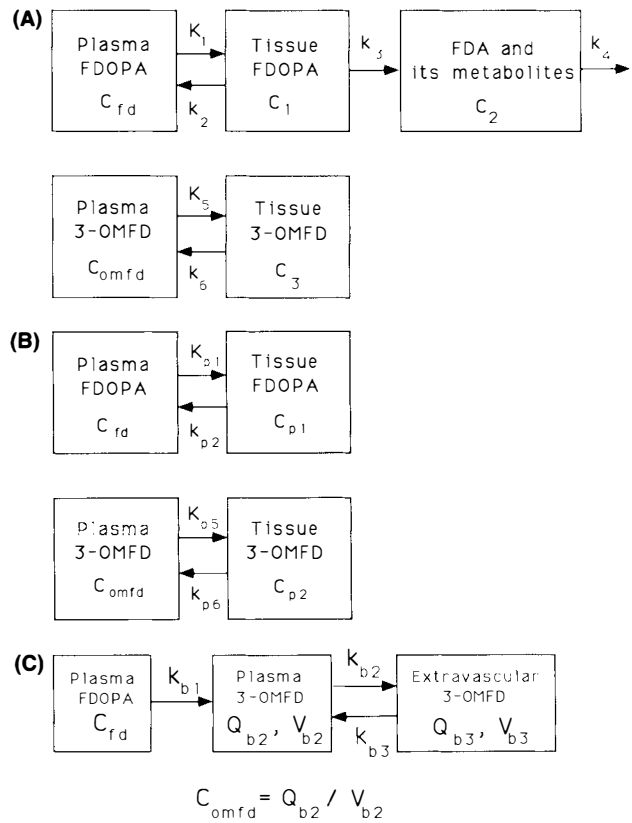

FIG. 2. Compartmental models for describing FDOPA kinetics in this study. **A:** Model for striatum consists of three separate compartments for tissue FDOPA, tissue FDA (and its metabolites), and tissue 3-OMFD. **B:** Model for cerebellum is similar to that of striatum, except that there is no compartment for FDA. **C:** Model for conversion of plasma FDOPA to 3-OMFD in the periphery consists of one compartment for plasma 3-OMFD and one for the extravascular pool. See text for explanation of symbols and abbreviations.

$$C_c(t) = K_{p1}C_{fd}(t) * \exp(-k_{p2}t) + K_{p5}C_{omfd}(t) * \exp(-k_{p6}t) + CBV \cdot C_{wb}(t) \quad (3)$$

Similarly, the time average cerebellar radioactivity corresponding to a PET scan from time t_1 to t_2 is

$$C_{cm}(t_1;t_2) = \frac{\int_{t_1}^{t_2} C_c(t)dt}{t_2 - t_1} \quad (4)$$

Model for plasma FDOPA and 3-OMFD

Since plasma 3-OMFD is a product of plasma FDOPA, the relationship between the two concentrations can be described by the compartment shown in Fig. 2C. In this model, k_{b1} is the unidirectional transfer rate constant from plasma FDOPA to the plasma 3-OMFD compartment. The extravascular 3-OMFD compartment communicates bidirectionally with the plasma 3-OMFD compartment with rate constants k_{b2} and k_{b3} as shown in the figure. The total radioactivities in the plasma and extravascular 3-OMFD compartments are denoted as Q_{b2} and Q_{b3}, respectively. The volumes of the two compartments are V_{b2} and V_{b3}. Based on this model, the kinetics of plasma FDOPA and 3-OMFD concentrations are related by the following differential equation:

$$\frac{d}{dt}Q_{b2}(t) = k_{b1}C_{fd} - k_{b2}Q_{b2} + k_{b3}Q_{b3}$$
$$\frac{d}{dt}Q_{b3}(t) = k_{b2}Q_{b2} - k_{b3}Q_{b3} \quad (5)$$

Note that $C_{omfd} = Q_{b2}/V_{b2}$, and by adding and subtracting $k_{b1}C_{omfd}$ ($= k_{b1}Q_{b2}/V_{b2}$) on the right-hand side of the first equation, one can obtain

$$\frac{d}{dt}Q_{b2}(t) = k_{b1}(C_{fd} + C_{omfd}) - \left(\frac{k_{b1}}{V_{b2}} + k_{b2}\right)Q_{b2} + k_{b3}Q_{b3}$$
$$\frac{d}{dt}Q_{b3}(t) = k_{b2}Q_{b2} - k_{b3}Q_{b3} \quad (6)$$

where $(C_{fd} + C_{omfd})$ is the total ^{18}F concentration in plasma (C_{f18}). By dividing both equations by V_{b2} (on both sides), the above equation can be expressed (Huang et al., 1991) as

$$\frac{d}{dt}C_{omfd}(t) = k_{b12}(C_{f18}) - (k_{b12} + k_{b2})C_{omfd} + k_{b3}C_x$$
$$\frac{d}{dt}C_x(t) = k_{b2}C_{omfd} - k_{b3}C_x \quad (7)$$

where $k_{b12} = k_{b1}/V_{b2}$ and $C_x = Q_{b3}/V_{b2}$. Solution of the above equation can give the plasma time–activity curve of 3-OMFD in terms of the total ^{18}F time–activity curve in plasma that is usually measured directly. In other words, if the fractions of 3-OMFD in plasma samples are assayed at a few time points, the parameter values of k_{b12}, k_{b2}, and k_{b3}, and the time–activity curve C_{omfd} can be determined by curve-fitting procedures (Huang et al., 1991). After the curve of $C_{omfd}(t)$ is determined, $C_{fd}(t)$ can be obtained as the difference between C_{f18} and C_{omfd}.

In the above derivation, it is assumed that there are no other labeled metabolites in plasma. While this is valid for FDOPA studies with carbidopa pretreatment, some other labeled metabolites (Melega et al., 1990*a*, 1991*b*) appear in plasma when carbidopa is not given. The majority of these metabolites are not expected to cross the BBB, owing to their hydrophilicity. However, they contribute to the total ^{18}F activity in the plasma samples. To account for this situation, the second and third compartments of Fig. 2C can be considered as for 3-OMFD and other labeled metabolites together (i.e., total non-FDOPA component). Equation 7 and the procedure described above can still be used directly to give the time–activity curve of FDOPA in plasma (i.e., C_{fd}). In this case, a (′) is added to the symbols of the rate constants to distinguish them from those for 3-OMFD alone. After the time–activity curve of FDOPA is obtained, Eq. 5 can be used to curve fit the 3-OMFD fractions to provide the time–activity curve of 3-OMFD by using estimated C_{fd} as the input function and considering Q_{b2} and Q_{b3} as for 3-OMFD only (i.e., excluding other labeled metabolites).

METHODS

Synthesis of FDOPA

FDOPA (specific activity 1–2 Ci/mmol) was synthesized following the procedure previously described (Luxen et al., 1990).

PET studies

Ten drug-free volunteers (age 21.8 ± 3.9 years) deemed normal by history and physical examination were recruited in accordance with the policies of the UCLA Human Subject Protection Committee. The volunteers were fasted for 4 h, and a dose of carbidopa (100 mg in four subjects; 250 mg in three; 0 mg in three) was given orally 60 min before the injection of FDOPA. Each subject was placed supine in a PET scanner (Siemens CTI 831) and a headholder was used to immobilize the head in a position to allow the whole brain to be covered by the 15 imaging planes (6.75-cm interplane separation) of the scanner. Subjects were told not to move during the study, were positioned in a comfortable posture, and were not spoken to during the study. Low ambient lighting and minimal machinery noise defined the environment. A transmission scan (using a ^{68}Ge ring source) was performed to provide

attenuation information for later attenuation correction of the emission scans.

A bolus of FDOPA (5 mCi) was injected intravenously over ~30 s and a sequence of PET scans (6 × 0.5 min, 4 × 3 min, 5 × 10 min, 3 × 20 min, total time of 125 min) was started concurrently. Arterial blood samples (~1 ml each) were taken at 0.16-min intervals for 2 min, 1-min intervals for another 3 min, and at gradually increased intervals until the end of the PET scan sequence. The blood samples were centrifuged and plasma taken for radioactivity counting in a well counter. The samples at 5, 10, 30, 60, and 120 min were also assayed biochemically by HPLC for separation of FDOPA, 3-OMFD, and other labeled metabolites (Melega et al., 1990*b*, 1991*b*).

In five separate human studies, the arterial blood samples were taken in duplicate for counting in well counter for ^{18}F activities in whole blood and in plasma. Hematocrits were also measured.

PET images were reconstructed with a Hann reconstruction filter (cutoff frequency 1.0 × Nyquist frequency) to give an in-plane spatial resolution of 8.4 mm full width at half-maximum and an axial resolution of 6 mm full width at half-maximum.

Regions of interest (~4–5 cm^2 in area on a cross-sectional plane of largest striatal area) were defined separately according to the apparent boundary of the structure on the emission images for the left and right striata (caudate and putamen), based on a summed image from 60 to 120 min. Regions of interest (~10 cm^2 in area) for the cerebellar hemispheres were similarly drawn, but were based on early images (1–10 min). These regions of interest were then applied to the serial PET images obtained at various scan times to give tissue ^{18}F time-activity curves of the corresponding regions. The curves from the left and right sides were averaged to give one striatal and one cerebellar time–activity curve for each study.

Data analysis

Plasma time–activity curves of FDOPA and 3-OMFD were obtained based on the model-fitting approach described in Theory, with the total ^{18}F time–activity curve in plasma used as the input function and the percentage 3-OMFD data from biochemical assay as the fitted measurements.

In the studies with both whole-blood and plasma ^{18}F measurements, the whole-blood time–activity curve was fitted by the following equation to estimate the partition coefficients of FDOPA and 3-OMFD in whole blood relative to plasma:

$$C_{wb}(t) = p_1 (1 - Hct)\, C_{fd}(t) + p_2\, C_{omfd}(t) \qquad (8)$$

where $C_{fd}(t)$ and $C_{omfd}(t)$ are, respectively, the time-activity curves of FDOPA and 3-OMFD in plasma as obtained from the model-fitting approach (Eq. 7); *Hct* is the measured hematocrit in peripheral whole blood; and p_1 (1 − *Hct*) and p_2 are the partition coefficients of FDOPA and 3-OMFD in whole blood relative to the plasma concentration. The hematocrit was included in the partition coefficient because the human red blood cell membrane is not very permeable to L-DOPA (Floud and Fahn, 1981).

The striatal time–activity curve for each study was fitted with the striatal FDOPA model described earlier (Fig. 2A and Eq. 2).The distribution volume of 3-OMFD in cerebral tissue was assumed to be uniform and equal to 1.0 (Horne et al., 1984; Doudet et al., 1990; Melega et al., 1991*b*). A fixed blood volume of 5% was assumed for striatal and cerebellar tissue regions (Phelps et al., 1979). The whole-blood radioactivity concentrations were calculated according to the following equation that assumed a hematocrit of 40% and accounted for the separate partition coefficients of FDOPA and 3-OMFD in blood:

$$C_{wb}(t) = p_1\,(0.6) C_{fd}(t) + p_2\, C_{omfd}(t) \qquad (9)$$

where p_1 and p_2 were the average of the estimates from the studies with both whole-blood and plasma measurements. For studies that contained labeled metabolites other than 3-OMFD (i.e., without carbidopa), the plasma component due to these metabolites was assumed confined to plasma (i.e., not entering the red blood cell) and was grouped together with $C_{fd}(t)$ in the above estimation of the whole-blood radioactivity concentrations.

The convergence of the model fitting was slow with large variability for the K_5 estimate. The fitting was thus performed with a constraint on the ratio of K_5 to K_1. A range from 0.5 to 3.0 of the constrained value was used for each striatal curve. The constrained value that gave the lowest total residual sum of squares of the 10 model fittings was used as a fixed value in other subsequent fittings. With the constraint on the distribution volume of 3-OMFD (i.e., $K_5/k_6 = 1$) and the K_5/K_1 ratio, there remained four variable parameters (K_1, k_2, k_3, and k_4) in the model fitting. Each striatal curve was also model fitted without k_4 (i.e., by setting k_4 equal to zero). The *F* test (Landaw and DiStefano, 1984; Bates and Watts, 1988) was used to examine if the model with k_4 gave a significantly better fit to the striatal tissue data.

The model fitting to the cerebellar time–activity curve was similarly performed (with the K_{p5}/K_{p1} ratio constrained to the K_5/K_1 value determined from striatal curves), except the cerebellar FDOPA model (Fig. 2B) was used. With the constraint on the distribution volume of 3-OMFD and the K_{p5}/K_{p1} ratio, there were only two variable parameters (K_{p1}, k_{p2}) in the model fitting. The effect of the total scan time on the reliability of various model parameters was examined by gradually reducing the length of the tissue curves in the model fitting from 120 to 55 min.

The effects of tissue heterogeneity on the measured striatal time–activity curve and on the parameter estimates were examined. Time-activity curves of various amounts of tissue mixture were simulated by appropriately averaging the striatal and cerebellar time–activity curves (assuming the time–activity curve in tissue adjacent to the striatum is similar to that of the cerebellum). The range examined was from −30 to +30% of the adjacent tissue contribution {i.e., (simulated curve) = $[C_{sm}(t) + pC_{cm}(t)]/[1 + p]$, with the p value ranging from −30 to +30%}. The negative p values correspond to the case of having some mixture effect corrected from the PET-measured striatal curve. The simulated activity curves were then fitted by the striatal model to examine the changes in the estimated parameter values.

A software package, BLD (Carson et al., 1981) for kinetic data modeling and simulation was used to perform all the model fittings in this study, using a weighted least-squares criterion and the Marquardt algorithm. The weightings used were inversely proportional to the variances of the measurements that were approximated as $0.01 \int C_{wb}dt/\Delta t + (C_t/\Delta t)$, where C_t was the measured

tissue radioactivity concentration, Δt was the scan time of the measurement, and the integral was over the scan time. The first term in the variance approximation was to account for errors and uncertainties in the estimation of the vascular radioactivity due to the blood volume in tissue. The coefficient 0.01 was chosen such that the first term was large in the early time when blood activity was high but became relatively insignificant in late times. Asymptotic values of the standard errors of the estimates were calculated from the covariance matrix of the estimates (Landaw and DiStefano, 1984; Huang et al., 1986).

RESULTS

Figure 3 shows the time–activity curves of total ^{18}F in whole blood and in plasma in a typical study. Figure 4 shows the fractions of 3-OMFD in plasma as determined by chemical assay. The model fitting to these measurements is also presented. Based on this model fitting, the separated time–activity curves of FDOPA and 3-OMFD along with the total ^{18}F curve in plasma are shown in Fig. 5. Table 1 summarizes the parameter values of the plasma FDOPA model (Fig. 2C) as determined by the model fittings to the chemically assayed plasma data in each subject. The partition coefficients of FDOPA and 3-OMFD in whole blood relative to plasma were found to be 1.01 ± 0.06 times ($1 - Hct$) and 1.08 ± 0.07, respectively.

Figure 6A shows the tissue time–activity curves obtained from serial PET images in a normal subject. As shown, the measured striatal and cerebellar curves were found to be fitted well, respectively, by the FDOPA models of Fig. 2A and B. The amounts of FDOPA, 3-OMFD, and FDA (plus its metabolites) in striatal tissue as estimated from the model fitting are also shown. The value of K_5 could not be determined uniquely from a single striatal curve (i.e., the model can fit the data equally well with a wide range of K_5 values). Without constraining the value of K_5, the convergence was slow, and in 3 of 10 cases, no convergence was obtained in 30 iterations (the maximal number of iterations selected for the present study). By fixing the ratio of K_5 to K_1 to various values in the fitting, the total residual sum of squares over the 10 studies is plotted in Fig. 7A and is shown to have a minimum near the value of 1.7. This value for K_5/K_1 was used in all subsequent model fits. The estimated values of the model parameters for each study are shown in Table 2. Based on the model fitting, the ratios of FDA (plus its metabolites) to total tissue radioactivity in striatum are 24 ± 7, 48 ± 9, 61 ± 6, and 67 ± 3%, respectively, at 10, 30, 60, and 120 min after FDOPA injection. These results are consistent with the biochemical data obtained in primates (Melega et al., 1991*a*).

The result of fitting the tissue curves of Fig. 6A, but with the model of zero k_4, is shown in Fig. 6B. The values of the parameter estimates for zero k_4 are summarized in Table 3 as a comparison with those allowing a variable nonzero k_4. With the F test, the fitting by the model with nonzero k_4 was found to be significantly better than that with zero k_4 in 8 of 10 studies [i.e., F value with (1,14) degrees of freedom was larger than the threshold value of 4.60 for $p < 0.05$].

The parameter estimates and the standard errors of the estimates are shown in Fig. 8 as a function of the total scan length. The estimates as well as their standard errors did not change significantly for total scan times longer than 90 min. Figure 7B shows the

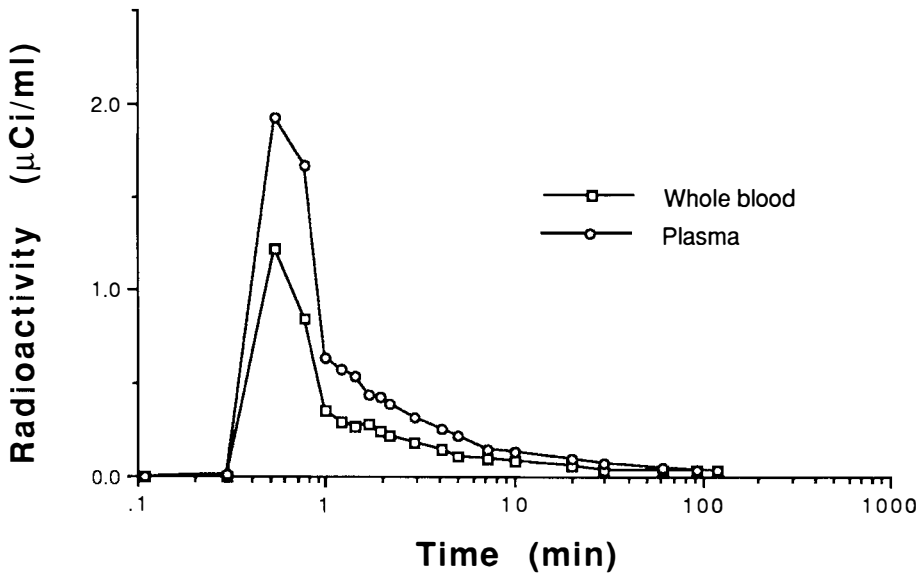

FIG. 3. Total ^{18}F time–activity curves in arterial blood and in plasma in a normal subject. The radioactivity concentration is higher in plasma than in whole blood at early times and approaches an equal level at late times.

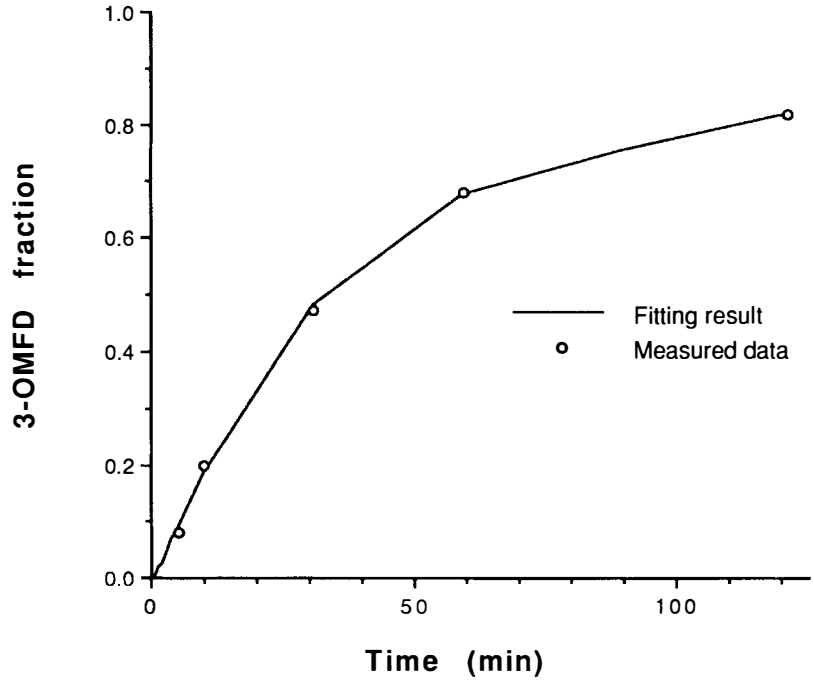

FIG. 4. 3-OMFD fractions of plasma radioactivity at different times after FDOPA injection in a normal subject. Carbidopa (250 mg) was given to the subject 60 min before the injection. The circles are data from biochemical assay using HPLC. The solid curve results from fitting the biochemical data with model of Fig. 2C. For abbreviations see the text.

sensitivity of the parameter estimates to the K_5/K_1 constraint. Although the value of the individual parameter changes, the overall uptake constant of FDOPA with respect to the plasma FDOPA concentration [i.e., $K_3 = K_1k_3/(k_2 + k_3)$] is insensitive to the exact value of the constraint used. The effect of tissue mixture on the estimated k_4 value is shown in Fig. 9. The value of k_4 estimate is seen to increase for larger amount of tissue mixture, but, over the range examined, the value of k_4 estimate is not affected by >25%. The estimated value of k_3 decreased for increased mixture (from 0.05/min to 0.026/min for mixture level of −10 to +30%). The estimated values of K_1 and k_2 were not affected over this range. However, from −10 to −30% mixture levels, the values of K_1, k_2, and k_3 increased by 1.2, 3.9, and 2.4 times, respectively. The large changes in the k_2 and k_3 estimates over this range were prob-

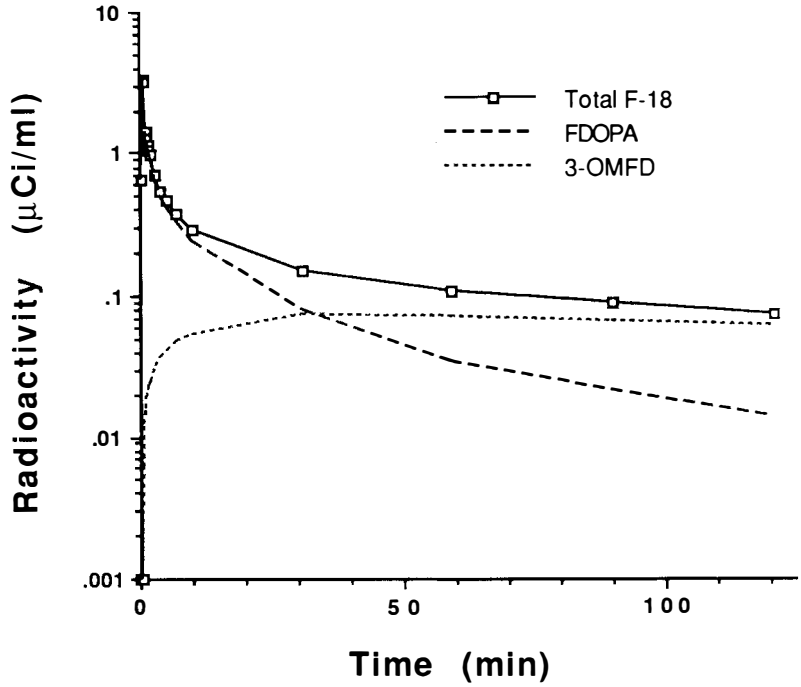

FIG. 5. Plasma time–activity curves after an intravenous bolus injection of FDOPA. Total ^{18}F activity measurements (squares) at various times were measured by a well counter. The curves for FDOPA (long dashes) and 3-OMFD (short dashes) were calculated based on Eq. 7 with the parameter values derived from the model fitting of Fig. 4. The amount of other labeled metabolites in plasma was negligible, because carbidopa (250 mg) was given to the subject before the study. For abbreviations see the text.

TABLE 1. *Rate constants for conversion of plasma FDOPA to plasma OMFD and other metabolites*

Subject no.	k_{b12}' (/min)	k_{b2}' (/min)	k_{b3}' (/min)	k_{b12} (/min)	k_{b2} (/min)	k_{b3} (/min)
1	0.0179	0.021	0.0051	0.0093	0.023	0.0138
2	0.0251	0.033	0.0056	0.0102	0.021	0.0076
3	0.0301	0.037	0.0055	0.0084	0.008	0.0[a]
4	0.0142	0.020	0.0051	0.0124	0.017	0.0050
5	0.0130	0.029	0.0142	0.0111	0.037	0.0167
6	0.0089	0.009	0.0[a]	0.0073	0.008	0.0[a]
7	0.0161	0.020	0.0065	0.0105	0.020	0.0129
8	0.0154	0.038	0.0136	0.0164	0.065	0.0214
9	0.0163	0.026	0.0103	0.0151	0.045	0.0225
10	0.0093	0.009	0.0050	0.0093	0.009	0.0051
Average	0.0166	0.024	0.0071	0.0110	0.025	0.0105
SD	0.0066	0.010	0.0043	0.0029	0.019	0.0082

Studies 1–3 were done without carbidopa; studies 4–7 were with 100 mg of carbidopa; studies 8–10 were with 250 mg of carbidopa.

The rate constants marked with primes are for FDOPA conversion to the combined pool of OMFD and other labeled metabolites; the symbols without the prime refer to the conversion to OMFD alone. Please see legend to Fig. 2C and text for symbols and abbreviations.

[a] Value was fixed in fitting.

ably due to an overcorrection of the mixture effect in the measured striatal curves.

DISCUSSION

The present results show that the model configurations of Fig. 2 describe well the tissue and plasma kinetics of FDOPA in humans as measured with PET. With these models, the component due to 3-OMFD (a labeled metabolite not related to cerebral tissue functions) can be separated from the total radioactivity in tissue, with the remaining component directly related to the transport and decarboxylation of FDOPA and the subsequent clearance of metabolites. From the kinetic data of an FDOPA PET study, the modeling approach is thus capable of providing information on the BBB transport, the decarboxylation, as well as the turnover rate of its metabolites in the striatum. The reliability and limitation of this extracted information are related to a multiple of factors that need to be carefully considered.

Separation of plasma curves

The separation of the plasma time–activity curve into FDOPA and 3-OMFD components in the present study was based on a modeling approach with an explicit model configuration of Fig. 2C for the conversion of plasma FDOPA to 3-OMFD. Based on this model, the conversion rate constant from FDOPA to 3-OMFD (k_{b12}) in the studies with carbidopa is comparable to that for the conversion to 3-OMFD plus other metabolites (k_{b12}'), indicating the fraction of plasma FDOPA converted in the periphery to labeled metabolites other than 3-OMFD is small, while for studies without carbidopa, the value of k_{b12}' is significantly larger than that of k_{b12}. The conversion rate constant to 3-OMFD alone (i.e., k_{b12}), however, does not correlate with the use of carbidopa. This indicates that carbidopa does not affect the conversion of FDOPA to 3-OMFD in the periphery, consistent with the biochemical information that carbidopa is a specific inhibitor of AAAD (Melega et al., 1990*a*). There is, however, a large intersubject variability in the conversion rate constant that prevents the use of a single fixed value for all subjects to simplify the study procedure. Although the conversion rate constant to 3-OMFD in the periphery does not depend on the carbidopa level, the plasma FDOPA level is higher with carbidopa than without. This along with a brain uptake mechanism for FDOPA that is not affected by carbidopa level (see discussion on BBB transport below) would give a higher striatal uptake of the tracer with carbidopa.

The model configuration of Fig. 2C may seem oversimplistic for describing the various transport/chemical pathways and organs in the body for FDOPA and 3-OMFD, but the model can fit the biochemically assayed data well. More complicated model configurations certainly can be formulated and would be more descriptive of the multiple processes involved. For the present study, however, only five plasma samples per study were assayed biochemically to give the activity percentages of FDOPA and its metabolites. The measurements will not allow us to formulate a model configuration much more complicated than the one of Fig. 2C. Extending the total study time and increasing the number of biochemical separations will improve this limitation. However, advancement in the biochemical assay to shorten the separation procedure is needed to make this practically feasible.

To investigate the effect of having inaccuracies in the model configuration for the separation of plasma FDOPA curves, the traditional method of using an ad hoc exponential function to fit the biochemically assayed percentage FDOPA data had also been used. Compared with those from the modeling approach, the exponential fitting gave an artifactual peak in the early part of the separated 3-OMFD curve in some studies (due to an underestimation of the percentage FDOPA fraction at early times), and the number of exponential terms needed to fit the data varies from study to study. In terms of the estimated model parameters of FDOPA in striatum, however, the effect was found to be extremely small as shown in Table 3. The use of the

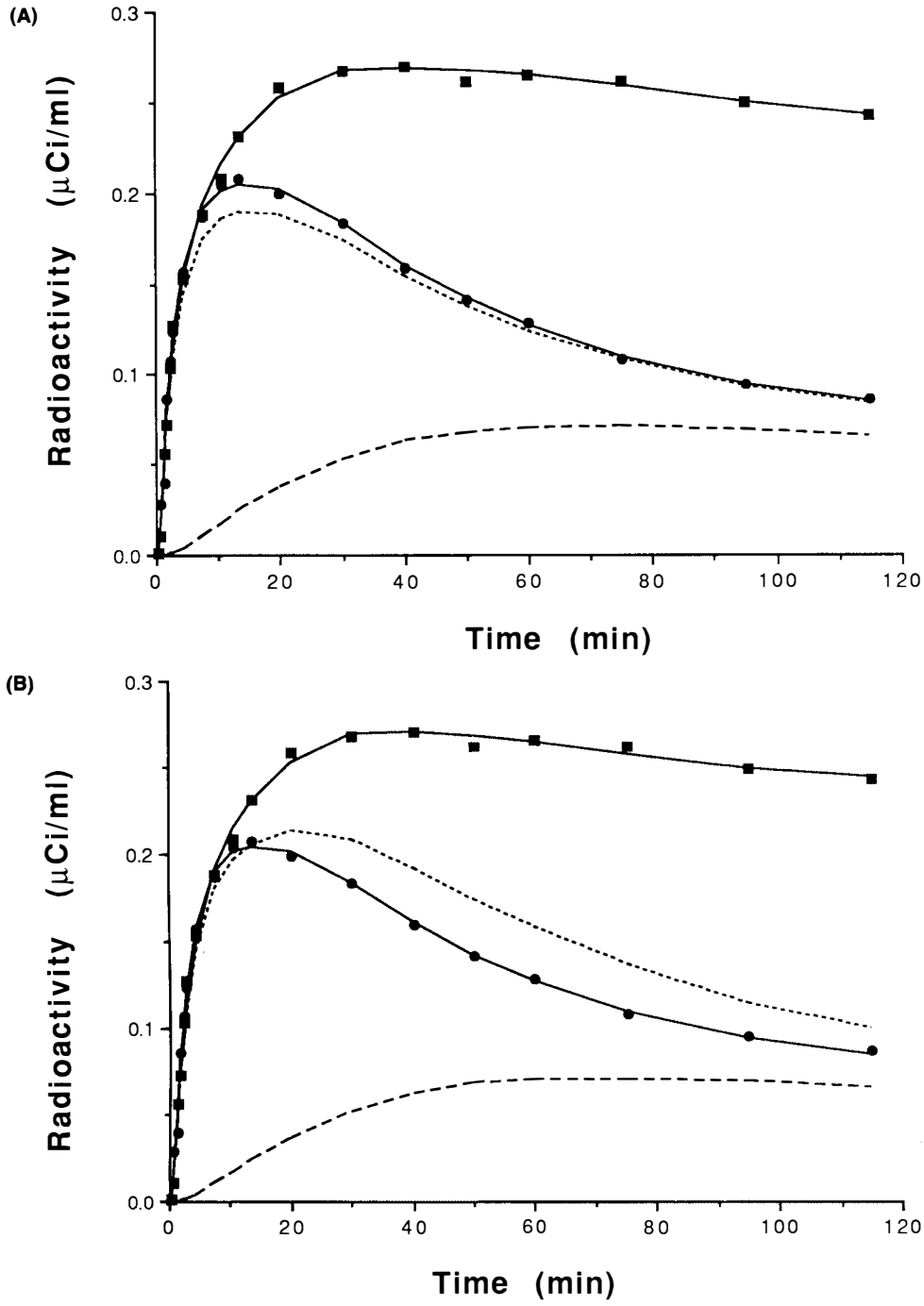

FIG. 6. A: Tissue time–activity curves (squares, striatum; circles, cerebellum) after an intravenous bolus injection of FDOPA. The solid curves are fits by models of Fig. 2A and B. The parameter value of k_4 in the model was allowed to vary in the model fitting. Based on the model fitting, the amount of 3-OMFD in striatal tissue is shown by the long dashed line. The short dashed line is the calculated amount of 3-OMFD and FDOPA in striatum. The space between the two dashed lines represents the amount of FDOPA in striatum; the space between the short dashed line and the solid curve for striatum represents the amount due to FDA and is metabolites in striatum. **B:** The same as in A, except that the value of k_4 was set to zero in the model fitting. The sum of 3-OMFD and FDOPA in striatum (short dashed line) is seen to be higher than that in cerebellum.

modeling approach also allows the plasma curve separation and the fitting of the tissue curves to be potentially integrated into a single estimation procedure.

The time–activity curve in whole blood obtained in this study does not parallel that in plasma. This is consistent with having different partition coefficients for whole-blood FDOPA and 3-OMFD relative to plasma concentrations. At early times when most plasma/blood activity is in the form of FDOPA, the radioactivity concentration ratio between whole blood and plasma is approximately equal to $(1 - Hct)$. This indicates that FDOPA is all in plasma and not in red blood cells. At late times (e.g., 120 min) when most plasma radioactivity is in the form of 3-OMFD, the whole blood/plasma ratio is ~1.0, suggesting that 3-OMFD permeates the red blood cell membrane. It is still unclear, however, what transport/chemical mechanisms account for their different permeability across the red blood cell

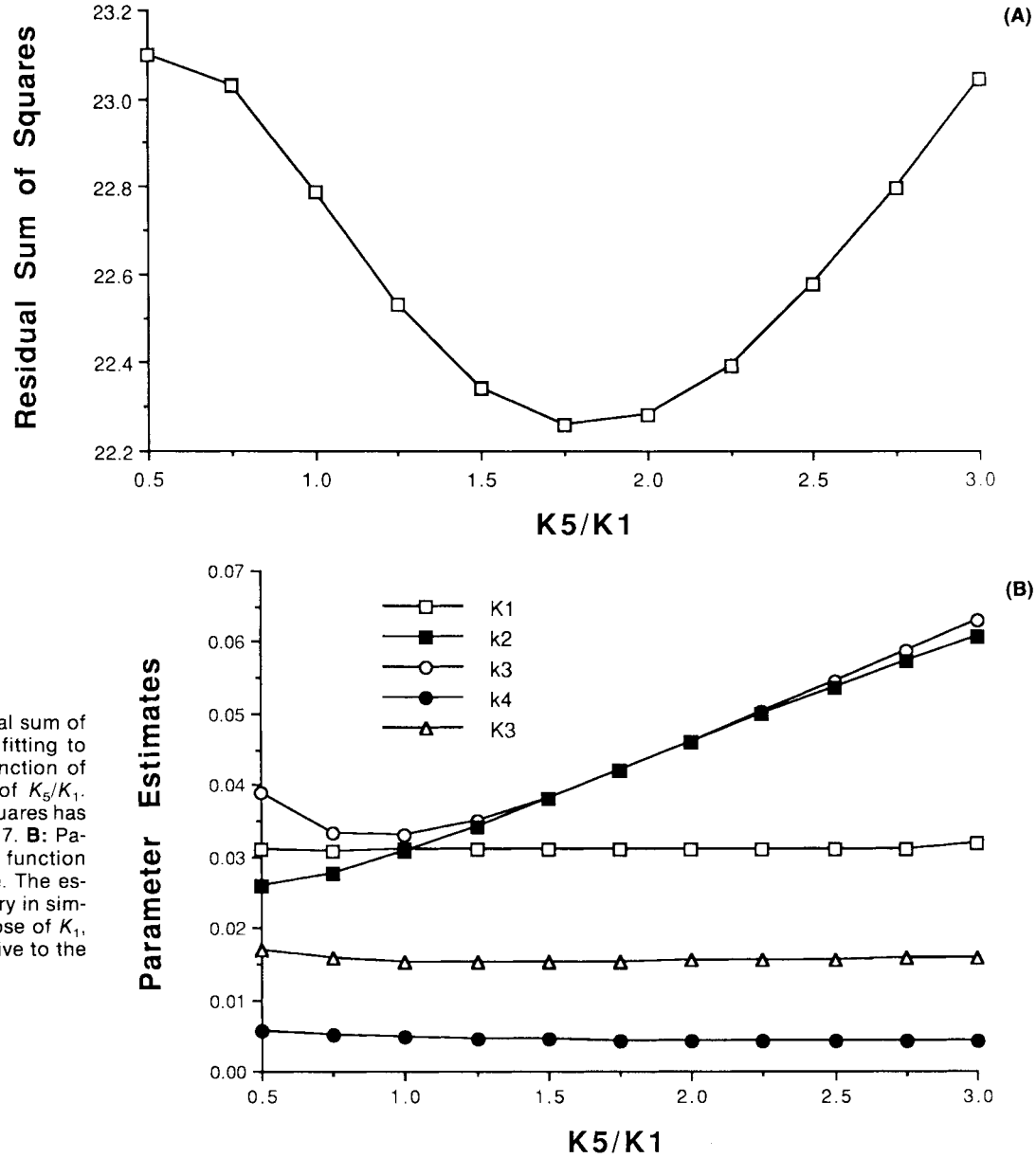

FIG. 7. A: Total residual sum of squares of the model fitting to striatal curves as a function of the constraint value of K_5/K_1. The residual sum of squares has its minimum around 1.7. **B:** Parameter estimates as a function of the constraint value. The estimates of k_2 and k_3 vary in similar fashions, while those of K_1, k_4, and K_3 are insensitive to the constraint value used.

membrane. This is currently under investigation in our laboratory. The difference in permeability between FDOPA and 3-OMFD can potentially be employed to separate the two labeled components in plasma, based on the measurements of whole-blood and plasma radioactivity concentrations similar to what has been used for [^{11}C]nomifensine studies (Salmon et al., 1990).

Estimation of vascular ^{18}F activity

In this study, the whole-blood time–activity curve was not measured in every study, but was estimated according to Eq. 9 from the separated plasma FDOPA and 3-OMFD curves. Effects of errors in the blood volume component on the estimated parameters were investigated by changing the assumed value of *CBV* from 0.05 to 0.08. The estimated values of k_2 and k_3 were affected the most with up to 30% decreases, but with parallel changes in these two parameters, resulting in <5% change in the K_3 estimate. All parameter estimates were insensitive to changes in the partition coefficients (p_1 and p_2) of FDOPA and 3-OMFD in blood. Also, changing the relative size of the variance component in the weightings (e.g., including/excluding radioactivity decay correction in the variance estimates) of the model fitting did not significantly affect the resulted estimates of the model parameters. In fact, the parameter estimates were not found to change much even with a completely different

TABLE 2. *Estimated FDOPA model parameters*

Study no.	K_1 (ml/min/g)	k_2 (/min)	k_3 (/min)	k_4 (/min)	K_{p1} (ml/min/g)	k_{p2} (/min)	K_3 (ml/min/g)	DV_s (ml/g)	DV_c (ml/g)
1	0.0285 (0.0014)	0.0511 (0.0129)	0.0662 (0.0145)	0.0069 (0.0004)	0.0335 (0.0024)	0.0383 (0.0062)	0.0161 (0.0006)	0.24 (0.05)	0.48 (0.02)
2	0.0303 (0.0012)	0.0450 (0.0077)	0.0441 (0.0070)	0.0050 (0.0004)	0.0383 (0.0014)	0.0640 (0.0029)	0.0145 (0.0006)	0.33 (0.04)	0.60 (0.01)
3	0.0461 (0.0022)	0.0457 (0.0086)	0.0376 (0.0088)	0.0060 (0.0008)	0.0453 (0.0022)	0.0587 (0.0033)	0.0208 (0.0008)	0.55 (0.09)	0.77 (0.02)
4	0.0302 (0.0016)	0.0458 (0.0097)	0.0394 (0.0082)	0.0021 (0.0006)	0.0296 (0.0013)	0.0424 (0.0023)	0.0139 (0.0006)	0.36 (0.06)	0.70 (0.02)
5	0.0285 (0.0020)	0.0362 (0.0117)	0.0349 (0.0150)	0.0043 (0.0013)	0.0305 (0.0009)	0.0440 (0.0017)	0.0140 (0.0017)	0.40 (0.12)	0.69 (0.01)
6	0.0302 (0.0012)	0.0309 (0.0067)	0.0313 (0.0103)	0.0040 (0.0010)	0.0420 (0.0025)	0.0639 (0.0048)	0.0152 (0.0014)	0.49 (0.11)	0.66 (0.02)
7	0.0302 (0.0010)	0.0261 (0.0046)	0.0264 (0.0078)	0.0029 (0.0010)	0.0326 (0.0005)	0.0495 (0.0010)	0.0152 (0.0014)	0.58 (0.12)	0.66 (0.01)
8	0.0307 (0.0008)	0.0340 (0.0036)	0.0201 (0.0037)	0.0009 (0.0009)	0.0388 (0.0028)	0.0762 (0.0069)	0.0114 (0.0009)	0.57 (0.06)	0.51 (0.02)
9	0.0333 (0.0013)	0.0453 (0.0086)	0.0502 (0.0094)	0.0052 (0.0004)	0.0315 (0.0012)	0.0426 (0.0021)	0.0175 (0.0007)	0.35 (0.05)	0.51 (0.02)
10	0.0251 (0.0019)	0.0497 (0.0192)	0.0611 (0.0203)	0.0060 (0.0006)	0.0294 (0.0017)	0.0587 (0.0045)	0.0138 (0.0007)	0.23 (0.06)	0.50 (0.02)
Average SD	0.0313 (0.0056)	0.0413 (0.0087)	0.0411 (0.0146)	0.0043 (0.0019)	0.0352 (0.0056)	0.0569 (0.0119)	0.0152 (0.0025)	0.41 (0.13)	0.63 (0.10)

Studies 1–3 were done without carbidopa; studies 4–7 were with 100 mg of carbidopa; studies 8–10 were with 250 mg of carbidopa. $K_3 = K_1k_3/(k_2 + k_3)$ is the decarboxylase rate constant in striatum with respect to plasma FDOPA concentration. $DV_s = K_1/(k_2 + k_3)$ denotes the distribution volume of FDOPA in striatum. $DV_c = K_{p1}/k_{p2}$ denotes the distribution volume of FDOPA in cerebellum. Values in parentheses for each study are the asymptotic standard errors of the parameter estimate. See text and Fig. 2 for model parameters and abbreviations.

weighting function of zero weightings in the first 3 min and a uniform weighting afterward.

Estimation constraints

In the present study, the distribution volume of 3-OMFD in cerebral tissue was assumed to be 1.0 ml/g, based on results obtained using 3-OMFD as the tracer (Doudet et al., 1990) and on biochemical data (Horne et al., 1984; Melega et al., 1991*a*). We have investigated the effects of potential errors in this assumed value in the model fitting by varying the value from 1.0 to 0.7 ml/g in 0.1-ml/g steps. The estimated values of k_3, K_3, and DV_s (distribution volume of FDOPA in striatum) were changed by +40, +20, and −20%, respectively. The estimates of K_1, k_2, and k_4, however, were not affected. For cerebellum, changing the distribution volume of 3-OMFD from 1.0 to 0.7 ml/g decreased the estimates of both K_{1p} and k_{2p} (by ~10 and 30%, respectively) and resulted in an increase of the distribution volume of FDOPA in cerebellum (DV_c) by ~20%. Also, the use of a distribution volume of 1.0 ml/g in the fitting usually resulted in the smallest residual sum of squares.

Given the noise level of the tissue measurements in the present study, the value of K_5 (forward BBB transport constant for plasma 3-OMFD) is unidentifiable (in the sense of having a unique and reliable estimate) from a single striatal time–activity curve. Over the 10 striatal curves obtained in the present study, however, the total residual sum of square has its minimum around $K_5/K_1 = 1.7$. In other words, if all 10 curves were model fitted together with the constraint that they have the same K_5/K_1 ratio, one would obtain an estimate of 1.7. Moreover, the minimal residual sum of square of the 10 cerebellar curves also occurs around the same value for K_{p5}/K_{p1}. The use of a common ratio is based on the reasoning that the ratio represents the relative transport efficiency of 3-OMFD and FDOPA in crossing the BBB and is expected to be less affected by measurement errors, such as the partial volume effect, which are different from study to study. In the investigation of the effect of the constraint on the model parameters, the estimated parameter values for k_2 and k_3 were found to be changed in a similar way, when the constraint was varied in the range from 0.5 to 3.0. The value of K_3 that repre-

TABLE 3. *Estimates of model parameters with variations in estimation procedures*

	Parameter estimate with nonzero k_4	Parameter estimate with $k_4 = 0$	Parameter estimate using input functions determined from exponential fittings
K_1	0.0313 (0.0056)	0.0283 (0.0051)	0.0305 (0.0038)
k_2	0.0413 (0.0087)	0.0228 (0.0048)	0.0401 (0.0115)
k_3	0.0411 (0.0146)	0.0124 (0.0041)	0.0394 (0.0122)
k_4	0.0043 (0.0019)	— —	0.0043 (0.0017)
K_{p1}	0.0352 (0.0056)	0.0352 (0.0056)	0.0345 (0.0049)
k_{p2}	0.0569 (0.0119)	0.0569 (0.0119)	0.0559 (0.0115)
K_3	0.0152 (0.0025)	0.0098 (0.0017)	0.0150 (0.0022)
DV_s	0.41 (0.13)	0.83 (0.18)	0.42 (0.15)
DV_c	0.63 (0.10)	0.63 (0.10)	0.63 (0.09)

See text and Table 2 for meaning of model parameters. Values in parentheses are standard deviations of estimates in 10 studies.

sents the total decarboxylation constant from plasma FDOPA as well as the K_1 and k_4 values, however, are not affected by the constraint (Fig. 7B).

Recently, Reith et al. (1990) have used a compartmental model to analyze FDOPA kinetics in rat studies. Although similar in configuration to the models examined here, their model does not account for the clearance of FDA and its metabolites in striatum. Also, different assumptions and constraints were used. In their model, the ratio of K_1/k_2 was assumed equal to K_5/k_6 and was the same for all cerebral structures. We have tested the use of equal K_1/k_2 and K_5/k_6 values in the estimation, and the effects on the parameter estimates are similar to those described earlier for using a distribution volume of 0.7 ml/g for 3-OMFD. The constraint of having the same ratio for different cerebral structures may not be valid for PET imaging studies, because of the dependency of the PET measured concentrations on the structural size that can affect differently the estimates of K_1 and K_5 for different structures (Hoffman et al., 1979; Mazziotta et al., 1981).

Effect of cerebral blood flow and BBB transport

Blood flow is not explicitly accounted for in the models of Fig. 2 for striatum and cerebellum, but is implicitly included in the parameters K_1 and K_5. The rate of FDOPA transport from arterial plasma to tissue is K_1C_{fd} according to the model of Fig. 2, while it is $F[1 - \exp(-PS/F)]C_{fd}$ based on the Renkin-Crone capillary model for the first-pass extraction of FDOPA in tissue, where F is blood flow and PS is the permeability–surface product of the BBB for the tracer. In other words, K_1 can be considered as a composite constant of $F[1 - \exp(-PS/F)]$. The K_1 value estimated in the present study is ~0.031 ml/min/g [comparable with the value of 0.037 ml/min/g recently reported for rat striatum (Reith et al., 1990)]. Assuming a blood flow value of 0.8 ml/min/g for the striatum, the first-pass extraction fraction is only 4% and the PS product is 0.032 ml/min/g, much smaller than the nominal blood flow to the tissue. In this case, one can show, by series expansion of the exponential term, that K_1 is approximately equal to PS and is thus insensitive to blood flow changes.

The permeability of FDOPA (and 3-OMFD) across the BBB is known to be mediated by the neutral amino acid carrier system in the BBB (Oldendorf, 1971). Since these channels are saturable (Oldendorf, 1971), the transport of FDOPA across the BBB (i.e., the value of K_1) is expected to be affected by the neutral amino acid level in plasma (Leenders et al., 1986*b*). In the present study, all the human subjects were fasted, and the plasma neutral amino acid levels were not expected to have deviated much from each other. This probably accounts for the relatively constant K_1 values among the subjects studied (Table 2). On the other hand, the subjects were given three different amounts of carbidopa before the study. The constancy of the K_1 value also suggested that carbidopa did not affect the transport of FDOPA across the BBB.

Decarboxylation rate of FDOPA in striatum

As compared to the Patlak graphical analysis that gives the uptake constant (K_3) from plasma FDOPA to tissue FDA (Martin et al., 1989), the present modeling approach can provide the value of k_3 [with a precision of about ±25% (Table 2)] that is specific to the decarboxylation of FDOPA to FDA. Although the absolute value of the k_3 estimate is somewhat dependent on the estimation constraints used in the model fitting, their consistent use should allow large changes in k_3 to be measured with the modeling approach. The present results show the k_3 value in normal subjects has an average value of 0.041/min that is comparable to that of k_2. This implies that about half of the FDOPA that normally crosses the BBB into striatum is decarboxylated, while the other half is transported back out of tissue. This, combined with the BBB forward transport constant K_1, gives a K_3 value of 0.015 ml/min/g.

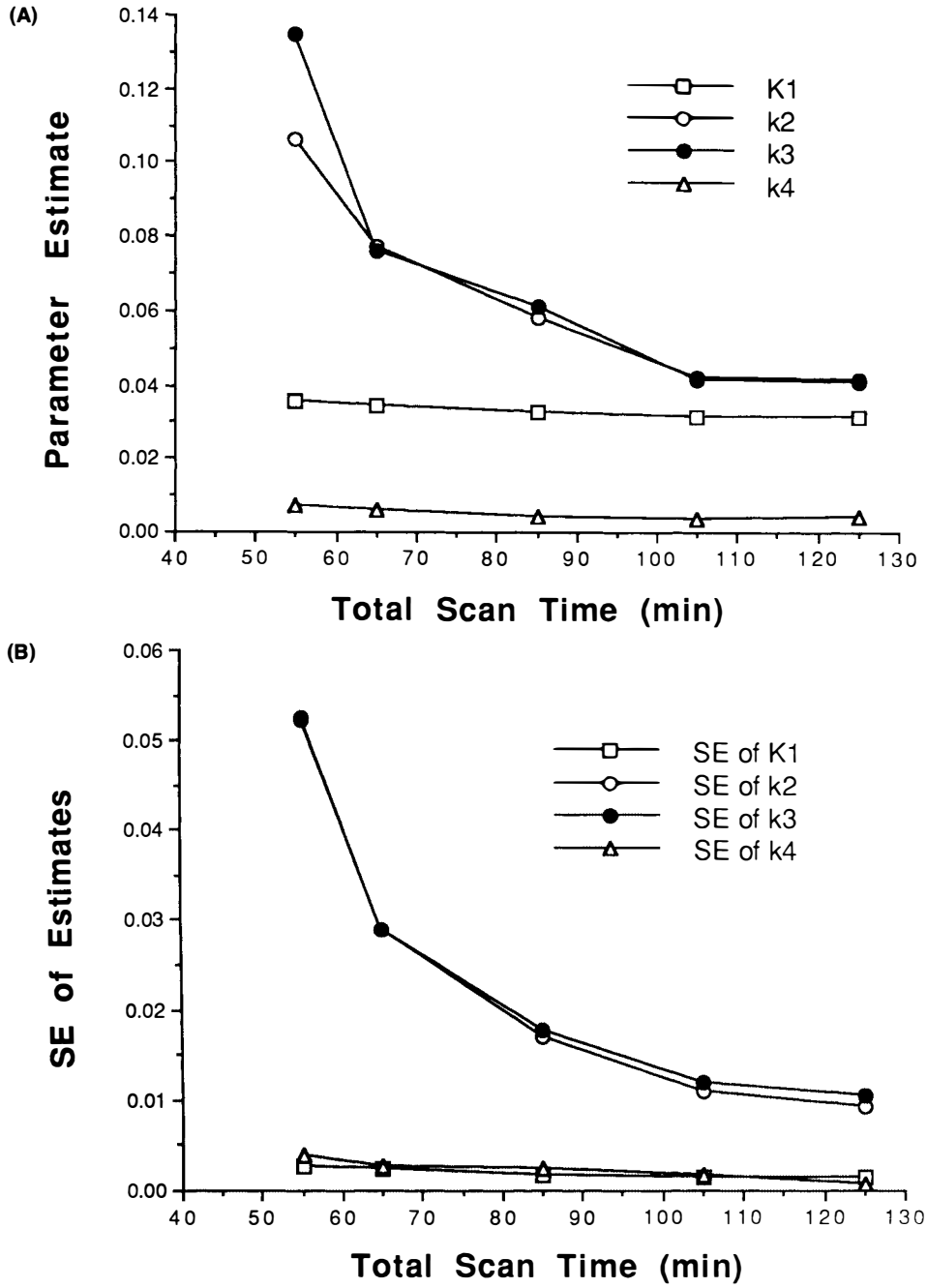

FIG. 8. Parameter estimates **(A)** and the standard errors of the estimates **(B)** as a function of the total scan time. As the total scan time is shortened to <90 min, the standard errors of the estimates increase and the values of the estimates diverge (except for K_1). The coefficient of variation of k_4 increases from 17% at 125 min to 58% at 85 min.

The value of K_3 has been measured before with Patlak analysis (Martin et al., 1989) to be ~0.8 ml/min/striatum in young adults. Assuming a unilateral striatal size of 13 ml in humans (Pasik et al., 1978), their reported value is equivalent to a value of 0.06 ml/min/g, much larger than the one obtained in the present study. It is not clear exactly what accounts for the difference, although multiple factors, including the differences in instrumentation and in data analysis, could be the potential error sources. The value of K_3 can also be deduced from the results reported recently in an abstract (Gjedde et al., 1990) to be ~0.011 ml/min/g. This value is comparable with the results of the present study. Similar values [~0.01 ml/min/g (Lindvall et al., 1990) and 0.017 ml/min/g (Tedroff et al., 1990)] for K_3 have also been reported by other laboratories. For these last two values, the total plasma ^{18}F radioactivity curve or the cerebellum curve was used as the input function in the calculation. Although the exact effect of not using the accurate input function on the K_3 value is unclear, the error is not expected to change K_3 by a factor of more than four. Additional studies are needed to reconcile the difference in values among different laboratories.

An interesting question about FDOPA as a tracer

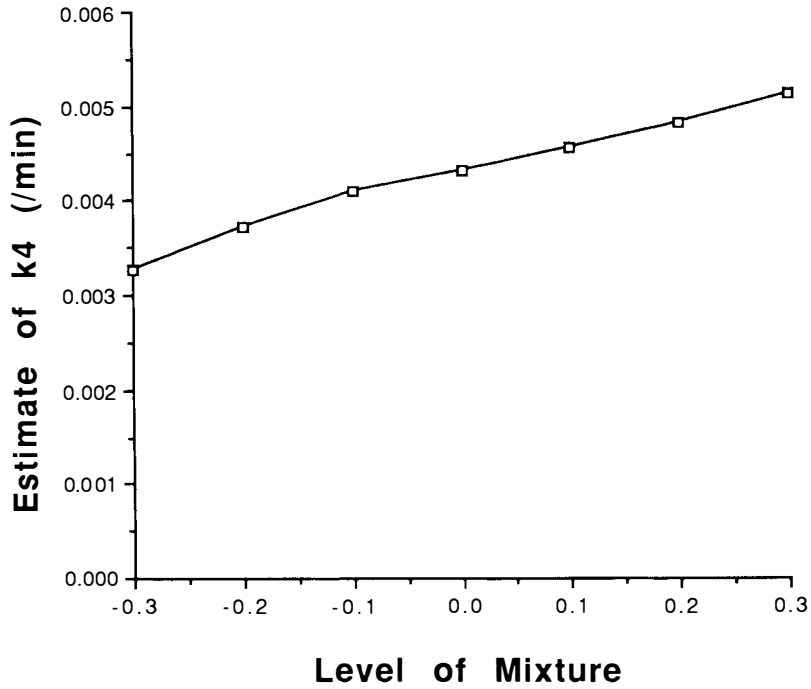

FIG. 9. Estimates of k_4 as a function of various amount of tissue mixtures. Zero level of mixture corresponds to the striatal curves obtained directly from positron emission tomography images. Positive level indicates additional amounts of tissue mixture from adjacent tissue (assumed to have the same kinetics as the measured cerebellar curve) have been added to the striatal curve before the model fitting. Negative level corresponds to the case of having some tissue mixture corrected. The k_4 estimates shown are averages of 10 human studies.

of L-DOPA decarboxylation is how the decarboxylation rate of FDOPA is related to the endogenous rate of dopamine formation. In normal dopaminergic neurons, dopamine is formed from tyrosine through hydroxylation (by tyrosine hydroxylase to L-DOPA) and decarboxylation (by AAAD to dopamine) reactions. It has previously been shown that tyrosine hydroxylation is the limiting reaction in this pathway and AAAD is in excess (Masserano and Weiner, 1983). One could argue that even if the decarboxylation rate constant (k_3) of FDOPA followed that of L-DOPA, the k_3 value alone does not necessarily give information about the rate of dopamine formation unless the endogenous L-DOPA level is also known. Since the endogenous L-DOPA level in tissue is believed to be small and to vary depending on pathology, the decarboxylation rate obtained from FDOPA measurements may not have much direct relevance to the rate of endogenous dopamine formation. This has been a concern about the interpretation of FDOPA PET studies.

If tissue AAAD is, however, in large excess, the measured value of k_3 is expected to be more dependent on the molecular diffusion and other cellular processes that transport FDOPA to the site of FDOPA decarboxylation (Hefti et al., 1981) and not dependent on the intrinsic chemical reaction rate of decarboxylation. In other words, in this case, the decarboxylation reaction is not the real limiting step, and the value of k_3 would be constant unless the amount of AAAD dropped to such a low level that the tissue L-DOPA level began saturating the enzyme and the decarboxylation reaction rate of FDOPA was affected by L-DOPA competition. This limiting case is more likely to occur when the neuronal function is immensely compromised in disease states as could occur in Parkinson's disease. Therefore, decrease in the k_3 value could indicate changes in the rate of dopamine formation and have relevance to neuronal function. Further investigations, including biochemical, neurological, and kinetic studies, are, however, needed to resolve this important issue.

Turnover rate of labeled metabolites

The inclusion of a clearance pathway (k_4) for the FDA and metabolites compartment in the model of Fig. 2A differs from other proposed FDOPA kinetic models (Reith et al., 1990). The central argument for not including k_4 is that the clearance of the metabolites from tissue would be slow and would not affect the estimates if neglected. The present results, however, show that ignoring k_4 would significantly affect the estimates of other parameters, especially that of K_3 (from 0.015 to 0.010 ml/min/g). Although the k_4 value estimated in normal subjects is not very large (corresponding to a half-time of 160 min) and does not cause a large deviation from a straight line in the Patlak plot, statistical test (F test) on the model fitting in the present study indicated the tissue kinetics are more consistent with a nonzero k_4 than without it. Also, as shown in Table 2 and illustrated in Fig. 6, if k_4 is neglected, the estimated distribution volume of FDOPA in striatum is larger than that in cerebellum. This is inconsistent

with the fact that FDOPA is decarboxylated in striatum but not in cerebellum, because by assuming the same BBB transport mechanism (forward and reverse) for striatum and cerebellum, one should expect the distribution volume of FDOPA in striatum to be smaller than that in cerebellum. Allowing a nonzero k_4, the result on the estimated distribution volume for striatum and cerebellum agrees well with this consideration (Table 2).

Owing to the limited spatial resolution of the PET images and the uncertainty in defining the exact boundary of the striatum, the measured striatal time–activity curve may consist of a component that is due to the adjacent tissue that does not have specific uptake of FDOPA (Huang et al., 1987). One may question whether this could have accounted for the nonzero k_4 estimate in the model fitting. The investigation of the tissue mixture addressed this question. Assuming that the adjacent tissue has kinetics identical to those in cerebellum, one can remove this component from the measured striatal curve. Figure 9 shows that by correcting this contribution from the adjacent tissue, the estimated k_4 value is reduced by no more than 25%. In other words, the mixture of kinetics from adjacent tissue, although having some effect on the estimated k_4 value, cannot account for the existence of the nonzero k_4 value. We have also applied the striatal model (with nonzero k_4) to cerebellar curves. In only 2 of the 10 studies did it give reasonable curve fitting that yielded a k_4 estimate of ~0.025/min. In the remaining eight studies, the fitting either gave negative or extremely large parameter estimates or did not converge after 30 iterations.

As shown in the accompanying article (Melega et al., 1991*a*), the concentration of FDA in primates at 60 min after FDOPA injection is much larger than those of its metabolites (mostly FHVA). This indicates that, in normals, the metabolic rate of FDA is quite slow. Since FDA does not cross cell membranes to any significant degree, its clearance from the tissue compartment must include FDA metabolism to FHVA. Therefore, the k_4 estimate represents a combination of the metabolic rate of FDA and the physical clearance rate of FHVA from tissue, although depending on the relative magnitude of the rate constants of the two processes, the estimate may reflect primarily either process. More direct biochemical and kinetic data on FDA and its metabolites in cerebral tissue, however, are needed to understand the exact significance of k_4. Also, it remains to be determined experimentally whether pathophysiological change in the human dopamine system will be reflected in changes in the estimated value of k_4.

Acknowledgment: The authors would like to thank the UCLA cyclotron staff for synthesizing the FDOPA compound used in this study; Mr. Ron Sumida and the UCLA PET scanner staff for performing the PET studies; and Drs. E. J. Hoffman, D. K. Mahoney, M. Dahlbom, A. R. Ricci, C. Selin, and G. Rosenquist for instrumentation, computer hardware, and software support. This work was partly supported by Department of Energy contract DE-AC0376-SF00012 and National Institutes of Health grants NS15654 and MH37916.

REFERENCES

Barrio JR, Huang SC, Phelps ME (1988) In vivo assessment of neurotransmitter biochemistry in humans. *Annu Rev Pharmacol Toxicol* 28:213–230

Bates DM, Watts DG (1988) *Nonlinear Regression Analysis and Its Applications.* New York, John Wiley

Boyes BE, Cumming P, Martin WRW, McGeer EG (1986) Determination of plasma [F-18]-6-fluorodopa during positron emission tomography: elimination and metabolism in carbidopa treated subjects. *Life Sci* 39:2243–2252

Calne DB, Langston JW, Martin WRW, Stoessl AJ, Ruth TJ, Adam MJ, Pate BD, Schulzer M (1985) Positron emission tomography after MPTP: observations relating to the cause of Parkinson's disease. *Nature* 317:246–248

Carson RE, Huang SC, Phelps ME (1981) BLD: a software system for physiological data handling and model analysis. *Proceedings of Fifth Annual Symposium on Computer Applications in Medical Care, Washington, DC, August, 1981,* pp 562–565

Chiueh CC, Burns RS, Kopin IJ, Firnau G, Chirakal R, Nahmias C, Garnett ES (1986) Determination and visualization of damage to striatal dopaminergic terminals in *N*-methyl-4-phenyl-1,2,3,6-tetrahydropyridine (MPTP)-induced parkinsonian monkeys by fluorine-18 labelled 6-fluoro-L-dopa and positron emission tomography. *Adv Neurol* 45:167–169

Cumming P, Boyes BE, Martin WRW (1987) The metabolism of [F-18]-6-fluoro-L-3,4-dihydroxyphenylalanine in the hooded rat. *J Neurochem* 48:601–608

Doudet DJ, Miyake H, Finn RT, McLellan CA, Aigner TG, Wan RQ, Adams HR, Cohen RM (1989) 6-[F-18]-L-Dopa imaging of the dopamine neostriatal system in normal and clinically normal MPTP-treated rhesus monkeys. *Exp Brain Res* 78: 69–80

Doudet DJ, McLellan CA, Adams HR, Miyake H, Finn RT, Cohen RM (1990) 6-(F-18)-Methoxydopa (F-3OM-DOPA) imaging in non-human primates. *J Nucl Med [Suppl]* 31:720

Firnau G, Garnett ES, Chirakal R, Sudesh S, Nahmias C, Schrobilgen G (1986) [F-18]Fluoro-L-dopa for the in vivo study of intracerebral dopamine. *Int J Radiat Appl Instrum* 37:669–675

Firnau G, Sood S, Chirakal R, Nahmias C, Garnett ES (1987) Cerebral metabolism of 6-[F-18]fluoro-L-3,4-dihydroxyphenylalanine in the primate. *J Neurochem* 48:1077–1082

Floud A, Fahn S (1981) L-DOPA (L-3,4-dihydroxyphenylalanine) uptake by human red blood cells. *Biochim Biophys Acta* 645:165–169

Freed CR, Breeze RE, Rosenberg NL, Schneck SA, Wells TH, Barrett JN, Grafton ST, Huang SC, Eidelberg D, Rottenberg DA (1990) Transplantation of human fetal dopamine cells for Parkinson's disease. *Arch Neurol* 47:505–512

Garnett ES, Firnau G, Nahmias C, Sood S, Belbeck L (1980) Blood-brain barrier transport and cerebral utilization of dopa in living monkeys. *Am J Physiol* 238:318–327

Garnett ES, Firnau G, Nahmias C (1983*a*) Dopamine visualized in the basal ganglia of living man. *Nature* 305:137–138

Garnett ES, Firnau G, Nahmias C, Chirakal R (1983*b*) Striatal dopamine metabolism in living monkeys examined in positron emission tomography. *Brain Res* 280:169–171

Garnett ES, Nahmias C, Firnau G (1984) Central dopaminergic

pathway in hemiparkinsonism examined by positron emission tomography. *Can J Neurol Sci* 11:174–179

Gjedde A, Reith J, Kuwabara H, Dyve S (1990) Determining dopa decarboxylase activity in the human brain in vivo: the complete fluoro-dopa model. *J Nucl Med* 31:720

Guttman M, Steele JC, Stoessl AJ, Peppard RF, Martin WRW, Walsh EM, Ruth T, Adam MJ, Pate BD, Tsui JKC (1987) 6-[F-18]Fluorodopa PET scanning in the ALS-PD complex of Guam. *Neurology* 37(suppl 1):113

Guttman M, Burns RS, Martin WRW, Peppard RF, Adam MJ, Ruth TJ, Allen G, Parker RA, Tulipan NB, Calne DB (1989) PET studies of parkinsonian patients treated with autologous adrenal implants. *Can J Neurol Sci* 16:305–309

Hefti F, Melamed E, Wurtman RJ (1981) The site of dopamine formation in rat striatum after L-dopa administration. *J Pharmacol Exp Ther* 217:189–197

Hoffman E, Huang S, Phelps M (1979) Quantitation in positron emission computed tomography. 1. Effect of object size. *J Comput Assist Tomogr* 3:299–308

Horne MK, Cheng CH, Wooten GF (1984) The cerebral metabolism of L-dihydroxyphenylalanine. *Pharmacology* 28:12–26

Huang S-C, Feng D, Phelps ME (1986) Model dependency and estimation reliability in measurement of cerebral oxygen utilization rate with oxygen-15 and dynamic positron emission tomography. *J Cereb Blood Flow Metab* 6:105–119

Huang S-C, Mahoney DK, Phelps ME (1987) Quantitation in positron emission tomography: 8. Effects of nonlinear parameter estimation on functional images. *J Comput Assist Tomogr* 11:314–325

Huang S-C, Barrio JR, Hoffman JM, Mahoney DK, Hawk TC, Melega WP, Luxen A, Grafton S, Mazziotta JC, Phelps ME (1989) A compartmental model for 6-[F-18]fluoro-L-dopa kinetics in cerebral tissues. *J Nucl Med* 30:735

Huang S-C, Barrio JR, Yu DC, Chen B, Gafton S, Melega WP, Hoffman JM, Satyamurthy N, Mazziotta JC, Phelps ME (1991) Modelling approach for separating blood time–activity curves in positron emission tomographic studies. *Phys Med Biol* 36:749–761

Landaw EM, DiStefano JJI (1984) Multiexponential, multicompartmental, and noncompartmental modeling. II. Data analysis and statistical considerations. *Am J Physiol* 246:R665–R667

Leenders KL, Palmer AJ, Quinn N, Clark JC, Firnau G, Garnett ES, Nahmias C, Jones T, Marsden CD (1986*a*) Brain dopamine metabolism in patients with Parkinson's disease measured with positron emission tomography. *J Neurol Neurosurg Psychiatry* 49:853–860

Leenders KL, Poewe WH, Palmer AJ, Brenton DP, Frackowiak RSJ (1986*b*) Inhibition of L-dopa uptake into the human brain by amino acids demonstrated by positron emission tomography. *Ann Neurol* 20:258–262

Leenders KL, Frackowiak RSJ, Lees AJ (1987) Progressive supranuclear palsy (PSP) studied with positron emission tomography. *Neurology* 37(suppl 1):113

Leenders KL, Aquilonius S-M, Bergstrom K, Bjurling P, Crossman AR, Eckernas S-A, Gee AG, Hartvig P, Lundqvist H, Langstrom B, Rimland A, Tedroff J (1988) Unilateral MPTP lesion in a rhesus monkey: effects on the striatal dopaminergic system measured in vivo with PET using various novel tracers. *Brain Rev* 445:61–67

Leenders KL, Salmon EP, Tyrell P, Perani D, Frackowiak RSJ (1989) Improved human brain 6-L-(F-18)-fluorodopa uptake by carbidopa pretreatment. *J Cereb Blood Flow Metab* 9(suppl 1):S419

Lindvall O, Brundin P, Widner H, Rehncrona S, Gustavii B, Frackowiak R, Leenders KL, Sawle G, Rothwell JC, Marsden D, Bjorklund A (1990) Grafts of fetal dopamine neurons survive and improve motor function in Parkinson's disease. *Science* 247:574–577

Luxen A, Perlmutter M, Bida GT, VanMoffaert G, Cook JS, Satyamurthy N, Phelps ME, Barrio JR (1990) Remote, semi-automated production of 6-[F-18]fluoro-L-dopa for human studies with PET. *J Appl Radiat Isot* 41:275–281

Martin WRW, Stoessl AJ, Adam MJ, Ammann W, Bergstrom M, Harrop R, Laihinan A, Rogers JG, Ruth TJ, Sayre CI, Pate BD, Calne DB (1986) Positron emission tomography in Parkinson's disease: glucose and dopa metabolism. *Adv Neurol* 45:95–98

Martin WRW, Palmer MR, Patlak CS, Calne DB (1989) Nigrostriatal function in humans studied with positron emission tomography. *Ann Neurol* 26:535–542

Masserano JM, Weiner N (1983) Regulation in the central nervous system. *Mol Cell Biochem* 53/54:129–152

Mazziotta JC, Phelps ME, Plummer D, Kuhl DE (1981) Quantitation in positron emission computed tomography: 5. physical–anatomical effects. *J Comput Assist Tomogr* 5:734–743

Melega WP, Hoffman JM, Luxen A, Nissenson CHK, Phelps ME, Barrio JR (1990*a*) The effects of carbidopa on the metabolism of 6-[F-18]fluoro-L-dopa in rats, monkeys and humans. *Life Sci* 47:149–157

Melega WP, Luxen A, Perlmutter MM, Nissenson CK, Phelps ME, Barrio JR (1990*b*) Comparative in vivo metabolism of 6-[F-18]fluoro-L-dopa and [H-3]L-dopa in rats. *Biochem Pharmacol* 39:1853–1860

Melega WP, Grafton ST, Huang SC, Satyamurthy N, Phelps ME, Barrio JR (1991*a*) L-6-[^{18}F]Fluoro-DOPA metabolism in monkeys and humans: biochemical parameters for the formulation of tracer kinetic models with positron emission tomography. *J Cereb Blood Flow Metab* 11:890–897

Melega WP, Hoffman JM, Schneider JS, Phelps ME, Barrio JR (1991*b*) 6-[F-18]Fluoro-L-dopa metabolism in MPTP-treated monkeys: assessment of tracer methodologies for positron emission tomography. *Brain Res* 543:271–276

Nahmias C, Garnett ES, Firnau G, Lang A (1985) Striatal dopamine distribution in parkinsonian patients during life. *J Neurol Sci* 69:223–230

Oldendorf WH (1971) Brain uptake of radiolabelled amino acids, amines and hexoses after injection. *Am J Physiol* 221:1629–1639

Pasik P, Pasik T, DiFiglia M (1978) The internal organization of the neostriatum in mammals. In: *The Neostriatum* (Divac I, Öberg RGE, eds), New York, Pergamon Press, pp 5–36

Patlak CS, Blasberg RG, Fenstermacher JD (1983) Graphical evaluation of blood-to-brain transfer constants from multiple-time uptake data. *J Cereb Blood Flow Metab* 3:1–7

Phelps ME, Huang S-C, Hoffman EJ, Selin CE, Kuhl DE (1979) Validation of tomographic measurement of cerebral blood volume with C-11 labeled carboxyhemoglobin. *J Nucl Med* 20:328–334

Reith J, Dyve S, Kuwabara H, Guttman M, Diksic M, Gjedde A (1990) Blood–brain transfer and metabolism of 6-[F-18]fluoro-L-DOPA in rat. *J Cereb Blood Flow Metab* 10:707–719

Salmon E, Brooks DJ, Leenders KL, Turton DR, Hume SP, Cremer JE, Jones T, Frackowiak SJ (1990) A two-compartment description and kinetic procedure for measuring regional cerebral [^{11}C]nomifensine uptake using positron emission tomography. *J Cereb Blood Flow Metab* 10:307–316

Tedroff J, Aquilonius S-M, Laihinen A, Rinne U, Hartvig P, Andersson J, Lundquist H, Haaparanta M, Solin O, Antoni G, Gee AD, Ulin J, Langstrom B (1990) Striatal kinetics of [C-11]-(+)-nomifensine and 6-[F-18]fluoro-L-dopa in Parkinson's disease measured with positron emission tomography. *Acta Neurol Scand* 81:24–30

Yu DC, Huang S-C, Barrio JR, Melega WP, Grafton S, Mazziotta JC, Phelps ME (1990) Investigation of a 6-[F-18]fluorodopa model for estimation of its kinetic parameters in human brain. *J Nucl Med* 31:865–866